

1 **Molecular basis of unidirectional information transmission in two-component**
2 **systems: lessons from the DesK-DesR thermosensor**

3 Sofía Lima¹, Juan Blanco², Federico Olivieri², Juan Andrés Imelio¹, Federico Carrión³,
4 Beatriz Alvarez⁴, Alejandro Buschiazzo^{1,5}, Marcelo Martí², Felipe Trajtenberg^{1,*}

5 **Affiliations:**

6 1 Laboratory of Molecular and Structural Microbiology, Institut Pasteur de Montevideo, Montevideo,
7 Uruguay

8 2 Departamento de Química Biológica e IQUIBICEN-CONICET, Facultad de Ciencias Exactas y Naturales,
9 Universidad de Buenos Aires, Buenos Aires, Argentina

10 3 Protein Biophysics Unit, Institut Pasteur de Montevideo, Montevideo, Uruguay

11 4 Laboratorio de Enzimología, Instituto de Química Biológica, Facultad de Ciencias, Universidad de la
12 República, Montevideo, Uruguay and Center for Free Radical and Biomedical Research, Universidad de la
13 República, Montevideo, Uruguay

14 5 Département de Microbiologie, Institut Pasteur, Paris, France

15 *For correspondence: felipet@pasteur.edu.uy

16 **Abstract**

17 Cellular signaling systems transmit information over long distances using allosteric
18 transitions and/or post-translational modifications. In two-component systems the
19 sensor histidine kinase and response regulator are wired through phosphoryl-transfer
20 reactions, using either a uni- or bi-directional transmission mode, allowing to build rich
21 regulatory networks. Using the thermosensor DesK-DesR two-component system from
22 *Bacillus subtilis* and combining crystal structures, QM/MM calculations and integrative

23 kinetic modeling, we uncover that: i) longer or shorter distances between the
24 phosphoryl-acceptor and -donor residues can shift the phosphoryl-transfer equilibrium;
25 ii) the phosphorylation-dependent dimerization of the regulator acts as a sequestering
26 mechanism by preventing the interaction with the histidine kinase; and iii) the kinase's
27 intrinsic conformational equilibrium makes the phosphotransferase state unlikely in the
28 absence of histidine phosphorylation, minimizing backwards transmission. These
29 mechanisms allow the system to control the direction of signal transmission in a very
30 efficient way, showcasing the key role that structure-encoded allostery plays in
31 signaling proteins to store and transmit information.

32 **Introduction**

33 Perception is a fundamental process that allows living organisms to adapt to highly
34 variable environments. Cells are equipped with a set of signaling pathways that
35 recognize specific signals, transmit and process the information to regulate different
36 cellular programs. Two-component systems (TCS) are relevant constituents of this
37 sensorial system in bacteria and archaea, also found in fungi and plants¹. TCSs are
38 usually composed of a sensor histidine kinase (HK), which detects a specific signal that
39 allosterically regulates their catalytic activities. Information is then transmitted further
40 downstream via phosphorylation of a specific response regulator (RR)², which acts as
41 the second component of the TCS pathway, executing the output response.

42 Upon the signal-dependent pathway activation, the HK autophosphorylates a
43 conserved His. A second reaction takes place in tandem, and the phosphoryl moiety
44 gets transferred to an invariant Asp within its cognate RR. Activation of the RR by
45 phosphorylation usually promotes its dimerization and subsequent binding to DNA, as

46 most RRs bear a DNA-binding domain responsible for exerting the effector response by
47 changing the expression of target genes³. In most TCSs, when the signal is absent, the
48 HK also promotes the dephosphorylation of the RR (*i.e.* acting as a phosphatase),
49 making of most HKs fascinating examples of paradoxical enzymes⁴. HK-mediated
50 P~RR dephosphorylation has been shown to be an extremely relevant process for
51 shutting down the system⁵ and preventing crosstalk⁶ *in vivo*. Interestingly, TCS
52 pathways have also evolved to increase their complexity by wiring additional
53 intermediate RR and His containing phosphotransferase proteins (HPT) domains that
54 ultimately build phosphorylation cascades, known as phosphorelays.

55 In the past few years several groups have made important contributions to the
56 understanding of the regulation of the activities of HK and RR^{3,7-14}, how their
57 components are functionally wired through specific protein-protein interactions¹⁵ and
58 how the signal is transmitted from the extra- to the intra-cellular space^{16,17}. Presently,
59 five HK families (HisKA, HisKA_3, HisKA_2, H-kinase_dim and HWE_HK) have been
60 recognized based on sequence clustering¹⁸; these families share many similarities at the
61 structural level^{9,11,13,19-21}. However, we are still far from understanding several
62 fundamental aspects of how HK-driven phosphorylation cascades transmit and process
63 information efficiently. For example, are phosphorylation/dephosphorylation futile
64 cycles minimized to avoid cell energy dissipation? If so, how is this accomplished from
65 a structural and mechanistic perspective? Or yet, how is the directionality of
66 phosphoryl-transfer reactions enforced, such that the P~RR species are accumulated,
67 or even to allow the connection with additional intermediate components to build richer
68 phosphorelays pathways?

69 Phosphoryl-transfer reactions occur by nucleophilic substitution. The electron-rich

70 oxygen of the RR's Asp carboxylate, attacks the phosphorus electrophile, substituting
71 the ϵ -nitrogen of the HK's His imidazole²² (Extended Data Fig 1). The directionality
72 issue should not be overlooked, since His phosphorylation is expected to be favored
73 over Asp phosphorylation considering available data on the hydrolysis of
74 phosphoramidate and phosphoanhydride compounds²³⁻²⁵. Dedicated mechanisms are
75 thus anticipated to surmount the uphill direction and ensure proper physiologic
76 behavior.

77 The TCS DesK-DesR from *Bacillus subtilis* is a thermosensor pathway that provides the
78 cells with a fast homeostatic response that maintains cell membrane fluidity²⁶. DesK is a
79 HisKA_3 HK that is activated upon cold shock. Phosphorylation at the invariant D54_{RR}
80 (Asp at position 54) of its cognate RR DesR triggers the adaptive response by activating
81 the expression of a fatty acid desaturase²⁷. The structural information available for this
82 system is unique. Several experimental structures of both components in different steps
83 of the signaling pathway, and adopting different conformations have been
84 elucidated^{7,9,28,29}. The catalytically active cytosolic and soluble region of DesK (DesKC)
85 can adopt at least three functionally and structurally different conformations:
86 autokinase, phosphatase and phosphotransferase states, involved in the
87 autophosphorylation, phosphoryl-transfer and dephosphorylation activities,
88 respectively. Based on the crystal structures of the DesK:DesR complex, and their
89 comparison to other TCSs, the distance between the phosphoryl-donor and -acceptor
90 residues (the HK His and RR's Asp, respectively) correlates with the systems'
91 directionality or degree of phosphoryl-transfer reversibility. Shorter distances predict a
92 tight transition states in the nucleophilic substitution reaction²², *i.e.* a pentavalent
93 bipyramidal transition state, and for still not understood reasons correlates with more

94 reversible phosphoryl-transfer reactions. Inversely, longer distances between reactive
95 residues imply loose transition states, *i.e.* a more dissociated planar trigonal
96 metaphosphate transition state, that correlate with irreversible P~His→Asp transfer
97 reactions⁷.

98 In the present work, to further understand how phosphoryl-transfer reversibility is
99 controlled in TCSs, quantum mechanics/molecular mechanics (QM/MM) calculations
100 were performed describing the phosphoryl-transfer (phosphoryl transfer from His to Asp
101 or Asp to His) and dephosphorylation reactions (phosphoryl-hydrolysis or transfer
102 reaction from Asp to a water molecule) using the DesK-DesR system. The crystal
103 structure of the DesK:DesR complex in the phosphatase state was refined to higher
104 resolution than that previously available, further supporting the QM/MM data. Critical
105 residues for the phosphotransferase and the phosphatase activities were pinpointed
106 utilizing structure-guided point mutants. Finally, an integrative structural and kinetic
107 model of the system was constructed, identifying key directionality determinants of the
108 phosphoryl-transfer reaction. Overall, evidence that the different HK enzymatic activities
109 are insulated from each other is provided, a pivotal element that ensures information is
110 efficiently transmitted in the right direction.

111 **Results**

112 **A hydroxyl anion is required for phospho-aspartate hydrolysis in the HK-mediated** 113 **phosphatase reaction**

114 To explore the mechanistic details of the dephosphorylation reaction in TCSs, the Free
115 Energy Profile of the DesK-DesR system was calculated using QM/MM-based steered
116 molecular dynamics. Calculations were based on an improved version of the crystal

117 structure of the DesK:DesR complex in the phosphatase state (PDB id: 7SSJ), used as
118 the starting species. The refinement of the previously reported structure was improved
119 by reprocessing the raw diffraction data³⁰ with now available algorithms that better
120 handle anisotropic diffraction³¹. The resolution could thus be extended to 2.52 Å in the
121 best direction, and 2.8 Å in the other two (Extended Data Table S1). The re-refined
122 electron density maps improved substantially. Among other features, Q193_{HK} (Gln at
123 position 193 of the HK) was now well defined in density, interacting with a water
124 molecule that coordinates the Mg²⁺ cation (Fig. 1a). An additional water molecule is now
125 clearly visible, hydrogen-bonded to the conserved T80_{RR} side chain (Fig. 1a), and well
126 positioned to interact with the attacking water molecule for phosphoryl hydrolysis.
127 Indeed, an unexpected electron density bulge coinciding with a Fourier difference peak
128 was observed near the phospho-mimetic BeF₃⁻ group, axially in line with the Be-O_{D54}
129 bond to D54_{RR} (Extended Data Fig 2). This feature is consistent with a water molecule
130 correctly placed to perform the nucleophilic attack, although limited data resolution
131 precludes conclusive modeling.

132 Our results showed that in order to simulate the P~Asp_{RR} hydrolysis reaction, the
133 attacking nucleophile has to be a hydroxyl anion, and not a water molecule. Attempts to
134 perform the reaction using a water molecule as the phosphate acceptor were
135 unsuccessful, even if the transferring phosphate was concertedly probed as the proton
136 acceptor. It must be stressed that the reaction center lacks a suitable residue that may
137 act as a base to deprotonate the reactive water. Therefore, the hydroxyl must be
138 formed in the bulk solvent. This observation is in accordance with the well-studied
139 Ras/GAP proteins mediating GTP hydrolysis, where a solvent-assisted mechanism has
140 indeed been put forward³².

141 The HK-mediated dephosphorylation reaction proceeds through a concerted
142 nucleophilic substitution mechanism, as evidenced by the changes at the interactomic
143 distance in the TS (transition state) zone (Fig. 1b and c), with an energy barrier of ~23
144 kcal/mol (Fig. 1b and c). The bond with the attacking water molecule occurs late in the
145 TS (defined as the higher energy state of the reaction pathway), implying a dissociative
146 mechanism with loose TS. The TS adopts the expected planar trigonal structure.
147 Q193_{HK}, which is bound to the Mg coordination sphere, remains hydrogen bonded to,
148 and accompanying the acceptor OH⁻ along the reaction, only to release it after the TS is
149 resolved, and the orthophosphate liberated as final product. The same QM/MM
150 calculation was performed in the absence of Mg²⁺, displaying a much higher energy
151 barrier. On the other hand, the calculated reaction without DesK, surprisingly showed a
152 similar profile (Extended Data Fig 3), suggesting that additional mechanisms should be
153 at play. Taken all the evidence together, the sidechain amide of the conserved Q193 on
154 the HK's α 1 helix, appears to assist in the reaction by placing the hydroxyl anion in a
155 catalytically ideal in-line attack position, which would otherwise be diverted by the
156 action of the phosphoryl oxygens³³.

157 **DesK:DesR phosphoryl-transfer follows a dissociative nucleophilic substitution** 158 **mechanism**

159 To test whether the difference in the distances between phosphoryl-acceptor and -
160 donor residues correlates with a looser or tighter phosphoryl-transfer TS between
161 phosphohistidine and aspartate, the free energy profiles of the reactions were
162 computed using QM/MM-based steered molecular dynamics using either a HK:RR or a
163 phosphorelay Hpt:RR type of complexes. First, to build the starting
164 phosphotransferase-competent state of the DesK:DesR complex, the crystal structure

165 of the DesKC_{H188E}:DesR_{REC}¹ complex was used (PDB id:5IUK)⁷, into which the
166 phosphorylated H188_{HK} was modeled by superimposing the crystal structure of
167 phosphorylated wild type DesK alone (PDB id:5IUM)⁷. The reaction could be nicely
168 simulated, exhibiting a low energy barrier (Fig. 2a, Table 1 and Extended Data Fig 4),
169 and confirming that the starting point is a good representation of the
170 phosphotransferase state.

171 The reaction starts with the phosphoryl moiety bound onto H188_{HK} and also
172 establishing a hydrogen-bond with Thr80_{RR} (Extended Data Fig 4b). The latter hydrogen
173 bond remained during the whole reaction. The TS shows the *en transfer* phosphoryl-
174 group adopting a planar trigonal structure (metaphosphate). Remarkably, the TS zone
175 shows a dissociative character. Although the reactive D54_{RR} got initially closer to the
176 phosphoryl group (Fig. 2a), the O-P distance stopped decreasing at ca. 2.8 Å (*i.e.* the
177 new covalent bond is not yet established) to then remains constant while the N-P bond
178 is stretched. Only after the donor N-P bond increased to 3.1Å (*i.e.* bond cleavage) the
179 D54_{RR} O-P bond was properly formed (Fig. 2a and Extended Data Fig 4b).

180 The role of the Mg²⁺ was assessed by calculating the free energy profile in the absence
181 of the metal cation. This resulted in a much larger energy barrier and unfavorably
182 positive reaction free energy (ΔG^0), similar to the calculated phosphoryl-transfer
183 reaction between isolated His and Asp residues in water (Table 1 and Extended Data
184 Fig 4a). The positive ΔG^0 for the isolated reaction is expected from a pure chemical
185 viewpoint, as described in the introduction. Consistently, phosphoryl-transfer reactions
186 using equimolar amounts of DesR_{REC}~P and DesKC, in the absence of Mg²⁺ showed
187 that the reaction proceeds slowly toward the His (Fig. 2b), spontaneously approaching

¹ REC: the phosphorylatable receiver domain of response regulators

188 maximum HK phosphorylation (*i.e.* hemiphosphorylation of the HK dimer)²⁹. This
189 indicates that the phosphoryl-transfer reaction itself is not completely abolished in the
190 absence of Mg²⁺, but the equilibrium is highly displaced toward the His.

191 Secondly, to compare *bona fide* HK:RR complexes with those of phosphorelay
192 pathways, similar free energy profile analyses were computed using the yeast
193 osmosensor phosphorelay complex Ypd1:Sin1 (Fig. 2). In this case the reaction showed
194 a more associative mechanism than for the DesK-DesR system, consistent with an
195 initial shorter distance between the phosphoryl donor and acceptor residues, and a
196 similarly small energy barrier of 7 kcal/mol (Table 1). The difference between the
197 product free energy (phosphorylated Asp) and the starting point (phosphorylated His) is
198 more positive in Ypd1:Sin1 as compared to the DesK-DesR system (Table 1 and
199 Extended Data Fig 4a) and similar to the His:Asp reaction in water (Table 1). This is an
200 important observation, consistent with our hypothesis of a correlation among
201 associative phosphoryl-transfer reactions, shorter inter-atomic distances, and the
202 chemical equilibrium displaced toward His phosphorylation, and *vice versa*. Altogether,
203 our results thus provide strong evidence that the experimental crystal structure of the
204 DesK_{H188E}:DesR_{REC} complex is a good mimetic of the phosphotransferase state and that
205 phosphoryl-transfer proceeds through a more dissociative mechanism or loose
206 transition state in DesK:DesR than in the phosphorelay.

207 **Highly conserved D189_{HK} and T80_{RR} residues are not essential for phosphoryl-**
208 **transfer**

209 The configuration of the phosphotransferase active site places the highly conserved
210 T80_{RR} at interaction distance with the covalently bound phosphoryl moiety of H188_{HK}.

211 This interaction was kept during the entire phosphoryl-transfer process in our QM/MM
212 calculations. To further analyze the relevance of T80_{RR} in the reaction, the HK-mediated
213 phosphorylation of T80A_{RR} (Fig. 3a) and T80S_{RR} (Extended Data Fig 5) mutants were
214 measured. In the *in vitro* assays, phosphoryl-transfer and desphosphorylation of the RR
215 are simultaneously taking place (biphasic curves). Intriguingly, DesK was able to
216 phosphorylate these two DesR mutants, showing phosphoryl-transfer reaction
217 comparable to wild type (Fig. 3b), thus indicating that T80_{RR} is not critical for the
218 reaction. QM/MM calculations of the phosphoryl-transfer reaction using the T80A
219 mutant, further suggest this residue is not essential (Table 1). Of note, T80A_{RR}, but not
220 T80S_{RR}, was unable to be phosphorylated using acetyl-phosphate as a phosphoryl-
221 donor (data not shown).

222 Concerning D189_{HK}, it can be predicted that this highly conserved acidic residue at
223 position H+1 (one residue C-terminal to the phosphorylatable His), is not involved in the
224 phosphoryl-transfer reaction. This is in contrast with the critical role that this residue
225 plays in subtracting a proton from the His δ N, increasing the nucleophilicity of the His in
226 the autophosphorylation reaction^{10,13,34,35}. In the phosphotransferase state, due to the
227 rotameric configuration of H188_{HK}, the δ N is oriented in a way that cannot interact with
228 D189_{HK}. Consistent with this view, reverse phosphoryl-transfer of a D189A_{HK} mutant
229 was not abolished (Fig. 3c).

230 **Phosphoryl-transfer reversibility is modulated by amino acid substitutions on the** 231 **RR**

232 QM/MM calculations suggested that, although a looser TS could be associated with a
233 shift in the equilibrium towards phosphorylation of the RR, when compared to the more

234 associative mechanism of the phosphorelay system, the ΔG^0 of the reaction was still
235 positive. Thus, on thermodynamic grounds, the transfer reaction appears to always
236 favor the phosphorylation of the HK. In this scenario, the following question emerges:
237 Have TCSs evolved additional mechanisms to deal with this energetic uphill? Three
238 different mechanism could be at play: i) dimerization of the phosphorylated form of
239 DesR could shift the equilibrium towards its phosphorylated state, especially
240 considering that its $\alpha 1\alpha 5$ surface is used for both RR dimerization and DesK-
241 interaction; ii) phosphorylated DesR might exhibit decreased affinity for DesK when
242 compared to the unphosphorylated species; and/or iii) in the absence of the sensor
243 domain, a shifted conformational equilibrium of DesK towards the phosphatase-
244 competent state would reduce the amount of available phosphorylatable His, given that
245 it is occluded inside the **D**imerization and **H**istidine phosphotransfer domain (DHp)⁷.
246 Since the interaction surfaces between DesK and DesR, comparing the HK's
247 phosphatase- and phosphotransferase-competent states, are very similar⁷, as are the
248 conformations of bound DesR, the second option of affinity changes seems unlikely.
249 Also, if DesR dimerization were to sequester the phosphorylated monomeric DesR
250 species out of equilibrium, this should also preclude DesK-mediated
251 dephosphorylation, which is clearly not the case. Thus, although dimerization could
252 contribute to the observed $P\sim\text{His}_{\text{HK}}\rightarrow\text{Asp}_{\text{RR}}$ directionality, it seems not be the main
253 driving force.

254 We reasoned that if the phosphatase/kinase equilibrium of DesKC is shifted towards
255 the former state, mutating residues that selectively affect DesR's interaction with the
256 phosphatase-competent state of the kinase only would induce a shift in phosphoryl-
257 transfer reversibility. To test this hypothesis two DesR mutants, R84A_{RR} and Q10A_{RR},

258 were tested. Residue R84_{RR} interacts specifically with DesK's D189_{HK}⁷, and due to the
259 gear-box mechanism⁹, the R84_{RR}:D189_{HK} interaction is disrupted in the
260 phosphotransferase state through the rotation of the DHp domain α -helices (Fig. 4a).
261 The R84A_{RR} substitution significantly reduced the dephosphorylation of the P~DesR
262 compared to wild type (Fig 3d), but the phosphoryl group still accumulates in DesR
263 (Figure 4b).

264 On the other hand, residue Q10_{RR} is inserted in a pocket generated at the interface
265 between the DHp and ATP binding domain (Figure 4c), a hallmark of the phosphatase
266 state³⁶. Remarkably, a Q10A_{RR} mutant showed a significant increase in phosphoryl-
267 transfer reversibility, with the phosphoryl moiety more evenly distributed between the
268 kinase and the regulator (Fig. 4d). Q10_{RR} is far from the phosphorylation site and was
269 previously highlighted as highly covariant with Q193 on the HK⁷. To rule out that
270 transfer reversibility of the Q10A_{RR} mutant is caused by a different positioning of DesR
271 in the phosphotransferase complex, potentially shortening the His_{HK}-Asp_{RR} distance, the
272 crystal structure of this complex was solved at 3.4 Å resolution. The structure clearly
273 indicated that the REC domain of DesR remains in the same position compared to the
274 wt (Extended Data Fig 6 and Table S1), especially not altering the His-Asp distance. The
275 observed change in phosphoryl-transfer reversibility is thus based on other reasons,
276 and directionality can be shifted by mutations at the response regulator that are far
277 from the phosphorylation site.

278 **A shifted HK conformational equilibrium minimizes phosphoryl-transfer reversal**

279 To better understand the key determinants of information transmission, a systems
280 biology and integrative approach was followed. Taking advantage that the different

281 functional states of DesK can be trapped³⁷, an experimental dataset comprising 770
282 measurements of the level of phosphorylation level in each protein (HK or RR) was
283 generated at different time points along the phosphoryl-transfer reaction assays. Two
284 types of reactions were analyzed, either starting with the phosphorylation of the HK
285 (Fig. 5c,d,e,f and g) or the RR (Fig. 5h and Extended Data Fig 7a,b,c,d, e and g). To this
286 end we used DesKC_{wt}, which lacks the transmembrane sensor domain, and was
287 previously shown to be deregulated^{9,38}. DesKC_{Q193A} was used to evaluate phosphoryl-
288 transfer with no confounding phosphatase activity. Q193_{HK} (H+5 position) is well
289 conserved in all HisKA_3 HKs and critical to keep phosphatase activity^{39,40}. DesKC_{DEST}
290 was also included, since this is a mutant that shifts the conformational equilibrium of
291 DesK towards the auto-kinase active state, by destabilizing the N-terminal coiled-coil⁸.
292 DesKC_{H188E} and DesKC_{H188V} are constructs that trap DesK in the phosphotransferase^{7,9}
293 and phosphatase state³⁸, respectively. In addition, wild type DesR_{REC} and the point
294 mutant DesR_{REC-Q10A}, were also tested. The analyzed reactions confirmed several
295 experimentally observed behaviors, such as the decrease in phosphatase activity of
296 DesKC_{Q193A} (Fig. 5e and Extended Data Fig 7c), or the increased phosphoryl-transfer
297 reversibility of DesR_{REC-Q10A} (Fig. 5d and f and Extended Data Fig 7b and d).

298 Different kinetic models were constructed and optimized, taking into consideration the
299 ensemble of available structural and biochemical data. The best-fitted model includes
300 19 free parameters (depicted in Fig 5a) and converged to a unique solution (Fig 5b).
301 Residuals to test the significance of the differences among alternative models were
302 rigorously monitored (see methods).

303 Several salient conclusions can be drawn from the optimized integrative model: i) the
304 equilibrium constant of the phosphotransferase reaction is directed towards His_{HK}

305 phosphorylation, as expected from our QM/MM calculations (K_{phos} (k_4/k_3) = 20.7, Table
306 1); ii) the kinetic rate constant ($k_5 = 0.227 \text{ s}^{-1}$) of the HK-mediated phosphatase activity
307 is 3 orders of magnitude higher than the intrinsic dephosphorylation rate of the RR ($k_9 =$
308 $3.87\text{E-}4 \text{ s}^{-1}$, autodephosphorylation); iii) the Q193A_{HK} substitution reduces the
309 phosphatase activity by 2 orders of magnitude ($k_5q = 6.082\text{E-}3 \text{ s}^{-1}$), but the activity is
310 not completely abolished; iv) the dissociation equilibrium constant of P~RR dimerization
311 is in the low μM range, and the Q10A_{RR} amino acid replacement increases this K_D by a
312 factor of 4 ($K_{D_RR_Q10A} = 1.442 \mu\text{M}$); v) the phosphatase/auto-kinase conformational
313 equilibrium of the HK is only slightly displaced towards the auto-kinase state; vi)
314 Q193A_{HK} and DesKC_{DEST} variant shift the phosphatase/auto-kinase equilibrium toward
315 the auto-kinase state; and, interestingly, vii) the auto-kinase/phosphotransferase
316 equilibrium is highly shifted towards the auto-kinase state, preventing phosphoryl back-
317 transfer.

318 The kinetic model also predicts that DesKC will interact with DesR mostly in a
319 phosphatase conformation. Isothermal titration calorimetry (ITC) data indeed confirmed
320 this hypothesis. DesKC associated to DesR with a 2:2 stoichiometry (two RR molecules
321 per HK dimer) as had been previously observed using a phosphatase-trapped mutant⁷.
322 Moreover, the relatively similar K_D values of the two independent binding sites was
323 consistent with a symmetric architecture as evidenced in the phosphatase configuration
324 (Extended Data Fig 8). The phosphotransferase configuration, due to its asymmetry,
325 exhibits substantially larger differences in the K_D values⁷. The kinetic model allows us to
326 make further predictions, such as a shift of the dimerization equilibrium in the DesR
327 Q10A_{RR} mutant, driving it towards the monomeric species (higher dissociation constant
328 of dimerization K_{DRRQ10} compared to wild type). Size-exclusion chromatography of

329 phosphorylated DesR-REC_{Q10A} indeed showed disturbed dimerization for this mutant
330 compared to the wild type protein (Extended Data Fig 9). Taking all the evidence from
331 the model together, we conclude that phosphoryl-transfer directionality is dictated by: i)
332 the auto-kinase/phosphotransferase conformational equilibrium, ii) the ratio between
333 the forward and reverse phosphoryl-transfer kinetic rates, and iii) the dimerization of the
334 P~RR.

335 **Discussion**

336 **A subtle displacement of the RR in the HK:RR interaction minimizes futile cycles**

337 Signal transduction pathways that use phosphorylation as a means to transmit
338 information use cellular energy by consuming ATP. In this context a key question is:
339 Have molecular machines evolved to minimize unwanted energy waste? There are
340 examples where energy dissipation is biologically relevant, for instance to deal with
341 noisy signaling and allow for adaptation⁴¹. In the case of TCSs, HK bifunctionality
342 confers robustness to the signaling process^{42,43}, but raises the question of how tightly it
343 must be regulated to avoid futile cycles and energy waste. In the present work we
344 described from first principles the HK-mediated dephosphorylation reaction of P~RR.
345 The crystal structure of the DesK:DesR phosphatase complex shows well-defined
346 density of key residues. That the phospho-mimetic BeF₃⁻ group bound to D54_{RR} shows
347 an unexpected bulge in the electron density suggest that instead a MgF₃⁻ (magnesium
348 fluoride) could be present as mimetic of the transition state⁴⁴ (Extended Data Fig 2). In
349 any case, the architecture of the reaction center in the X-ray structure is perfectly
350 consistent with the QM/MM calculations. The HK favors hydrolysis of the P~Asp by
351 organizing the active site within the RR, assisting with its glutamine in position H+5 in

352 the correct placement of the attacking hydroxyl anion. The interaction between the HK
353 in the phosphatase conformation and the phosphorylated RR promotes the opening of
354 the RR active site, exposing the phosphorylation site^{7,28}. According to our kinetic model,
355 the dephosphorylation of the RR is accelerated by the HK by 3 orders of magnitude
356 compared to the intrinsic autodephosphorylation reaction. Moreover, in the absence of
357 the conserved Q193_{HK} (Q193A substitution), the reaction is 2 orders of magnitude
358 slower compared to wild type HK. This modest acceleration and the effect of Q193
359 mutation is consistent with the proposed role of Q193_{HK}. The QM/MM calculations of
360 the dephosphorylation reaction in the presence or absence of the HK are similar,
361 implying that the acceleration promoted by the HK is likely gained through lowering the
362 entropy of the Michaelis complex. Analogous mechanisms have been put forward after
363 extensive studies of the Ras/Ras-like small GTPase family of proteins. In the case of
364 Ras, a GTPase activating protein (GAP) accelerates the reaction by several orders of
365 magnitude⁴⁵. The active site is very similar to the reaction center conformed between
366 the HK and the RR in TCSs (Extended Data Fig 10). GAP binding to Ras induces a
367 significant loss of entropy of the Gln, which was proposed to be critical in the GTP
368 hydrolysis reaction mechanism³².

369 When the HK is stabilized in its phosphotransferase conformation, to avoid futile cycles
370 the dephosphorylation of P~RR must be minimized. From a structural point of view,
371 even though differences in the HK active site are observed comparing its phosphatase
372 and phosphotransferase conformations, the position of Q193_{HK} is unchanged and the
373 conformation of the RR is almost identical⁷. Then, why is there no significant
374 phosphatase activity? An explanation can be uncovered by superimposing the
375 DesK:DesR phosphatase and phosphotransferase complexes. There is a small but

376 significant shift (approximately 1 Å) in the position of the RR. This movement, in the
377 phosphatase state, brings the phosphoryl-group and the Mg²⁺, with its entire
378 coordination sphere, closer to Q193_{HK} (Extended Data Fig. 11). Hence, Q193_{HK} comes
379 now within interaction distance with a water molecule of the Mg²⁺ coordination sphere,
380 properly placed to position the attacking hydroxyl anion. The ~1Å shift of the RR is
381 driven by a set of interactions between the REC domain and the HK ATP binding
382 domain, that are only available in the phosphatase state. In contrast, in the
383 phosphotransferase state, Q193_{HK} is not ordered, as evidenced by the electron density,
384 which is not well defined (Extended Data Fig 11). Collectively, our data suggest that
385 interactions involving secondary interfaces in the phosphatase state, more precisely
386 between the REC and ATP binding domain, guide the correct placement of the RR to
387 favor dephosphorylation. In the absence of this interaction, the RR is held farther apart
388 and thus not promoting the phosphatase reaction.

389 **Insulation of HK activities as an information-driving mechanism**

390 The higher energy of the mixed anhydride O-P bond on the P~Asp compared to the N-
391 P phosphoramidate in P~His²⁵, which is in turn higher than the anhydride O-P bond of
392 ATP⁴⁶, imposes an uphill energy barrier that the system must overcome to promote RR
393 phosphorylation. A shift in the phosphoryl-transfer reaction equilibrium according to the
394 distance between nucleophile and leaving group amino acids could be possible,
395 considering the position of the Mg²⁺ cation. The relative position of the cation changes
396 with respect to the HK, in different complex geometries. Our QM/MM calculations of
397 phosphoryl-transfers along looser or tighter TS, suggest that changing the distance
398 between the donor and acceptor residues can indeed setup different ΔG of the
399 reaction. Nevertheless, the ΔG is always positive in the P~HK→RR direction, so that

400 additional mechanisms are at play.

401 The structural model of the DesK-DesR system (Fig. 6a) suggests that the proper
402 accumulation of P~RR could be reached by: i) P~RR dimerization; ii) a reduction in
403 binding affinity to the HK when the RR is phosphorylated; and iii) through regulation of
404 the conformational equilibrium of the HK, making the phosphotransferase conformation
405 unlikely. According to the integrative kinetic model, the binding affinity of the HK to the
406 RR in phosphorylated and non-phosphorylated states of the latter, and either in the
407 phosphatase or phosphotransferase state of the HK, is unchanged. This is consistent
408 with all the experimental information, in particular the similarity of the phosphatase and
409 phosphotransferase binding areas at the HK:RR interface. Moreover, a decrease in the
410 affinity to the phosphorylated RR would also imply an inconsistent scenario where the
411 HK in the phosphatase state would be unable to interact with it. P~RR dimerization
412 does compete with HK binding, and the observed effect of the Q10A_{RR} mutant shows
413 that disturbing this equilibrium indeed results in a more reversible phosphoryl-transfer.
414 However, too tight a dimerization would also preclude HK-dependent and independent
415 dephosphorylation, which are constraints that need to be considered.

416 From our kinetic model, the parameters that contribute the most to the directionality
417 are: the ratio between the kinetic rates of the phosphotransferase along its forward and
418 reverse directions, and the conformational equilibrium between the HK's auto-kinase
419 and phosphotransferase states (Extended Data Fig 12). By moving the reactive His
420 closer or farther apart in the reaction center, the ΔG might be modulated due to the key
421 contribution of the Mg²⁺ cation at the beginning of the reaction, stabilizing the phospho-
422 His in case the distance is short enough (Fig. 6b). This is in agreement with the ΔG
423 calculated for the isolated His to Asp phosphoryl-transfer reaction in water (Table 1),

424 suggesting that in an associative mechanism the influence of the Mg^{2+} in shifting the
425 equilibrium towards Asp phosphorylation is lower. The solvent-occluded position of the
426 His inside the DHp core of the HK in the phosphatase conformation⁷ should minimize
427 reversibility as well. Mutants that shift the phosphatase/auto-kinase equilibrium should
428 be more reversible. We did not observe such effect when we tested $DesK_{DEST}$ (Fig. 5
429 and Extended Data Fig 7). On the other hand, our finding that the equilibrium between
430 the auto-kinase and phosphotransferase conformations was shifted against the latter,
431 which is the only competent state able to participate in the phosphoryl-transfer
432 reaction, also explains why the His is not accessible anymore (Fig. 6c). From a
433 structural point of view it appears that phosphorylation favors the phosphotransferase
434 state by triggering a conformational rearrangement. The highly conserved R235 and
435 K242 in HK helix a2 are well positioned to interact with the phosphoryl-group on the
436 reactive H188. This interaction likely pulls the a2-helix toward the a1-helix, breaking the
437 symmetric organization of the DHp and favoring the phosphotransferase state (Fig. 6d).
438 A tight non-covalent interaction between the guanidinium group of the Arg with the
439 phosphate⁴⁷ could provide the necessary energy to promote this somehow unfavorable
440 conformational transition.

441 The unexpected conformational equilibrium uncovered by our kinetic model also
442 indicates that the system is tuned to maximize signal transmission efficiency. In other
443 words, in the presence of the specific signal, HK activation promotes a shift in the
444 phosphatase/kinase conformational equilibrium towards the latter. However, depending
445 on the kinase/phosphotransferase conformational equilibrium and intracellular protein
446 concentrations, HK autophosphorylation might be inhibited by its the interaction with
447 the RR in the phosphotransferase state. Our kinetic model predicts that there is a

448 narrow window of the kinase/phosphotransferase equilibrium in which the system can
449 accumulate phosphorylated RR, and requires that in the absence of phosphorylation,
450 the phosphotransferase state of the HK is inaccessible (Extended Data Fig 13).

451 Taking all together, we conclude that the sensor domain controls the on/off switch by
452 changing the auto-kinase/phosphatase transition. But, the auto-
453 kinase/phosphotransferase equilibrium guarantees that the information cannot go
454 backwards. Finally, our findings might also be extrapolated to phosphorelay pathways,
455 in which different mechanisms could allow these systems to be more or less reversible,
456 by tuning the Asp-His distance, the dimerization of the phosphorylated effector RR, or
457 additional elements like local physicochemical properties in the immediate surroundings
458 of the P~Asp that were not considered in this work.

459 **Methods**

460 ***Classical (MM) Simulations***

461 All molecular dynamics simulations were performed using the AMBER suite package of
462 software⁴⁸. Classical force field parameters for aminoacids were obtained from the
463 ff14SB force field, whereas force field parameters for phosphorylated residues (phospho-
464 Asp and phospho-his) were generated with the Antechamber module of the AMBER
465 suite, after geometry optimization and RESP charge derivation at the HF/6-31G* level
466 with Gaussian g09, revision D.01⁴⁹. For each simulation, the equilibration protocol
467 consisted of 200-cycle runs of minimization with a 100 (kcal/mol)/Å² restraint constant
468 applied to the protein in order to relax the solvent structure, followed by a 1000-cycle
469 energy optimization in which the restraint was removed to avoid initial unfavorable
470 contacts. The system was then slowly heated to 300 K during a 1 ns simulation, with

471 the Berendsen thermostat. Finally, pressure was equilibrated at 1 atm over 1 ns, to let
472 the system reach the proper density. For all simulations we used the periodic boundary
473 condition approximation, with the Ewald summation method with a 10 Å cutoff for
474 nonbonded interactions, and the SHAKE algorithm for all hydrogen-containing bonds.
475 Final production 10 ns MD simulations were performed at 300 K using the Langevin
476 thermostat and a 2 fs time step, from which the last structure was selected for QM-MM
477 simulations.

478 ***Hybrid (QM-MM) Simulations***

479 All DFT QM/MM calculations in this work were performed with the SANDER(AMBER)
480 program and the QM(DFT)/MM implementation called LIO⁵⁰ using the PBE functional
481 and a DZVP gaussian basis set. All relevant parts of the computation of LIO are ported
482 to GPU, obtaining an improvement on the performance, including exchange and
483 correlation, Coulomb, and QM/MM coupling terms^{51,52}.

484 For the phosphotransfer reactions, the QM region consisted of 70 atoms (Extended
485 Data Fig 14), including both donor and acceptor amino acids (His/Asp), the magnesium
486 ion and its whole coordination sphere (sidechain of D9_{RR} and D54_{RR}, backbone carbonyl
487 of E56_{RR}, two water molecules, and the phosphate) and a total of 8 H-link atoms at each
488 corresponding boundary. For the phosphatase reaction the QM region is the same but
489 with the donor His replaced by a hydroxyl anion.

490 ***Multiple Steered Molecular Dynamics protocol***

491 To study both the phosphotransfer and the phosphatase reaction mechanisms, we
492 used a multiple steered molecular dynamics (MSMD) strategy, combined with
493 Jarzynski's relationship to determine the corresponding Free Energy Profiles. This

494 strategy has already been shown to be useful in previous works from our group for
495 phosphoryl transfer reactions^{35,53,54}. Briefly, in MSMD the system is driven “multiple”
496 times along the selected reaction coordinate under nonequilibrium conditions, by
497 applying an external force, and for each individual trajectory, the work performed by the
498 external force is computed. Finally, multiple works are exponentially averaged using
499 Jarzynski’s relationship to obtain the free energy profile. In the present work we first
500 performed 5 ns of conformational sampling at the reactive/product equilibrium
501 geometries using standard QM/MM Molecular Dynamics. This was followed by 10
502 independent MSMD simulations (starting from corresponding initial structures each
503 separated by 500 ps) which were run for approximately 2 ps using a 0.001 ps time step,
504 resulting in a pulling speed of 2 Å/ps. The force constant used was 200 kcal.mol⁻¹.Å⁻².
505 All the reaction mechanisms were simulated in both forward and reverse directions, and
506 in each case the reported free energy profile corresponds to the optimal combination of
507 both, as usually done when applying this strategy. The reaction coordinate for each
508 profile was always the difference between the donor atom to P and P to acceptor
509 (attacking atom) distances (See Extended Data Table S2 for values)

510 ***Cloning, Protein Expression and Purification***

511 Cloning and protein purification were performed as described previously^{7,9,28}.
512 Briefly, plasmid pQE80_DesKC_{DEST} was generated by subcloning DesKC_{DEST} from
513 pHPKS/Pxyl-desKDEST⁸ into pQE80-DesR through PCR amplification using primers
514 DesK_BamHI_F (CACGGATCCAGCAAGGAGCGCGAACGACTTG) and DesK_Sall_R
515 (TCCTGGTCTGACTTA TTTTGAATTATTAGGAATTGC), BamHI and Sall digestion, and
516 ligation. pQE32-DesKC_{Q193A} was constructed using primers DesKQ193A
517 (GATACGCTTGGGGCAAAGCTTT CTC) and DesK_Rev

518 (GAATTATTAGGAATTGCCATGGTAAGCTTGGTC) by RF cloning⁵⁵. pQE80_DesR-
519 REC_{Q10A} was generated by similar procedure using DesR_Q10A_F (5'-
520 GTATATTTATTGCAGAAGATGCGCAAATGCTGCTGG-3') DesR-REC_R (5'-
521 GCTTCGCTGTATAAGTCCTCCATCAG-3'). Recombinant proteins DesKC, DesR-REC
522 and derived mutants were expressed as N-terminally His6-tagged fusions in *E. coli*
523 strain TOP10F'. The last purification step was a size exclusion chromatography (HiLoad
524 16/60 Superdex 75 preparation grade column; GE) equilibrated with 20 mM Tris-HCl pH
525 8.0, 0.3 M NaCl (SEC buffer). All proteins were concentrated to ~10 mg/mL and stored
526 at -80°C.

527 ***Autodephosphorylation, Phosphotransferase and Phosphatase Assays***

528 Phosphorylation of DesKC was performed by incubating purified DesKC with 10 mM
529 ATP and 10 mM MgCl₂ for an hour at 24°C in SEC buffer. The reaction mix was then
530 loaded in a Superdex75 10/300 column (GE Healthcare) equilibrated in with a solution
531 containing the SEC buffer. To obtain phosphorylated DesR_{REC} and DesR_{REC-Q10A}, each
532 pure protein (~600 μM) was autophosphorylated using 50 mM acetyl phosphate and 30
533 mM MgCl₂ for an hour at 24°C, in the same buffer. Reactions were stopped by adding
534 EDTA (50 mM), and loaded into a Superdex75 10/300 column (GE Healthcare)
535 equilibrated in buffer SEC. The peak corresponding to the dimeric species was selected
536 for further analysis.

537 The phosphotransfer assay was started by incubating P~DesKC (wild type or mutant) at
538 a concentration of 26 μM (concentration of the monomeric species) with equimolar
539 amounts of DesR_{REC} (wild type or mutant) in reaction buffer (20 mM Tris-HCl pH 8.0, 0.3
540 M NaCl and 5 mM MgCl₂) for 30' at 24°C. At different time points the reactions
541 were stopped by adding SDS-PAGE sample buffer with 2.5 mM of DTT. Excess

542 DTT was blocked with 40 mM iodo-acetamide and loaded in a Phos-tag SDS-PAGE, as
543 described before²⁸. Coomassie blue-stained gels were scanned and quantification was
544 done by densitometry using ImageJ⁵⁶.

545 Auto-dephosphorylation of P~DesR_{REC} (wild type or mutants) was performed as above,
546 incubating P~DesR_{REC}, at different protein concentrations, in Reaction buffer at 24°C.
547 On the other hand, DesK promoted DesR dephosphorylation was done by incubating
548 26 μM P~DesR_{REC} in the presence of DesKC (wild type or mutants) at 26 μM (except for
549 DesK_{C_{H188V}} that different concentrations were tested) in Reaction buffer at 24°C.
550 Reactions were stopped at different time points and loaded in a Phos-tag SDS-PAGE
551 as described above.

552 ***Protein Crystallization, Data Collection and Model Building***

553 The DesK_{C_{H188E}}:DesR_{REC-Q10A} complex was prepared by mixing 300 μM DesK_{C_{H188E}} and
554 165 μM DesR_{REC-Q10A} in a buffer containing Tris-HCl 20 mM pH 8.0, 0.3M NaCl, 20 mM
555 MgCl₂ and 5 mM AMP-PCP (non-hydrolysable analogue of ATP). The complex
556 crystallized in a mother liquor containing 20% (w/v) PEG 3350 and 0.35 M tri-potassium
557 citrate⁷. Protein drops were setup by mixing 2 μL of protein plus 2 μL of mother liquor.
558 Cryo-protection was achieved by quick soaking in 20% (w/v) PEG 3350, 0.35 M tri-
559 potassium citrate, 5 mM AMP-PCP, 25% (v/v) glycerol, and 20 to 150 mM MgCl₂ + 5
560 mM BeF₃⁻.

561 Single crystal X-ray diffraction was performed in a copper rotating anode home source
562 (Protein Crystallography Facility, Institut Pasteur de Montevideo). Diffraction data was
563 processed with autoProc⁵⁷ and structure was solved by molecular replacement using
564 each molecule of 5IUJ⁷ as search probe in Phaser⁵⁸. We reprocessed the X-ray

565 diffraction data from 5IUN by merging two dataset from the same crystal in autoPROC.
566 Model building was done in Coot⁵⁹ and refinement in Buster⁶⁰. Validation was done
567 throughout and towards the end of refinement using MolProbity tools⁶¹. Visualization of
568 protein models and structural analyses and figure rendering were performed with
569 Pymol⁶². Software for data processing, structure determination and analysis was
570 provided by the SBGrid Consortium³⁰.

571 ***Analytical Size Exclusion Chromatography***

572 To analyze phosphorylation-triggered dimerization of Q10A_{RR} substitution, recombinant
573 purified proteins dimeric phosphorylated DesR_{REC} and DesR_{REC-Q10A} Dimeric species
574 were obtained as described above and degree of phosphorylation for both proteins was
575 determined by Phostag SDS-PAGE. Then 100 μ L of 100 μ M protein, with a degree of
576 phosphorylation of 60%, was loaded in a Superdex75 10/300 column (GE Healthcare)
577 equilibrated with a buffer containing 20 mM Tris-HCl pH 8.0, 0.3 M NaCl and 10 mM
578 MgCl₂ and run at 0.5 mL/min.

579 ***Kinetic Model of the DesK-DesR System***

580 Several kinetic models were constructed taking into consideration biochemical,
581 structural and biophysical information from previous work^{7,9,28}. We considered models
582 with two or three functional states of DesK, in the latter case assuming the kinase state
583 to be different from the phosphotransferase state. The autophosphorylation reaction
584 was not included in the model, since all the reactions were performed in the absence of
585 ATP or ADP. In addition, we tested models in which the binding of DesK might occur
586 with identical or different affinity when DesR is phosphorylated or not. We also tested a
587 simplified model where we discarded the second binding site for DesR in the

588 phosphotransferase state of DesK. The best-fitted model is depicted in Fig. 5. Each
589 model was constructed as custom scripts in Matlab R2020a (MathWorks Inc.),
590 consisting in a set of differential equations that describes each reaction, conformational
591 rearrangement (like kinase/phosphotransferase transition) or interaction between
592 proteins. The model equations were solved numerically using the ode15s solver.
593 Parameters were globally optimized by minimizing the sum of squared residuals (SSR)
594 of the full dataset with the simplex search method as implemented in fminsearch with
595 boundaries (John D'Errico (2021). fminsearchbnd,
596 fminsearchcon ([https://www.mathworks.com/matlabcentral/fileexchange/8277-
597 fminsearchbnd-fminsearchcon](https://www.mathworks.com/matlabcentral/fileexchange/8277-fminsearchbnd-fminsearchcon)), MATLAB Central File Exchange). Given the complexity
598 of the parameter space, an exhaustive search was performed, starting from 800000
599 different initial conditions, uniformly distributed in the multidimensional space. The
600 confidence intervals of the fitted parameters were estimated using lsqcurvefit in Matlab.
601 In order to compare different kinetic models the standard deviation of the SSR was
602 calculated by bootstrap. Models that showed a SSR worse than 10 standard deviations
603 with respect to the best model were discarded.

604 ***Isothermal Titration Calorimetry***

605 Isothermal titration calorimetry (ITC) assay was performed on a VP-ITC (Microcal VP-
606 ITC (Malvern Panalytical) as previously described⁷. Briefly, titration was carried out at
607 15°C in a buffer containing 20 mM Tris-HCl pH 8.0, 0.3 M NaCl, 10 mM MgCl₂ and 0.5
608 mM AMP-PNP. The concentration of dimeric DesKC was 15 μM and DesR_{REC} 380 μM.
609 Raw data were analyzed with NITPIC v1.2.7^{63,64} and integrated binding isotherms were
610 fitted to a model with two independent sequential sites using SEDPHAT v12.1b⁶⁵. Plots
611 including corrected thermograms, fittings of binding isotherms and residuals were done

612 with GUSI⁶⁶.

613 **Data availability**

614 The X ray structures presented have been deposited in the wwPDB with
615 accession codes 7SSJ (DesK-DesR complex in the phosphatase state) and 7SSI
616 (DesK-DesR_{Q10A} complex in the phosphotransfer state). Raw X ray diffraction data
617 corresponding to each one of these structures are publicly available at SBGrid Data
618 Bank (<http://data.sbgrid.org>) as dataset entries XXX.

619 **Acknowledgements**

620 We thank Joaquin Dalla Rizza, Nicole Larrieux and Analia Lima for assistance in protein
621 purification, crystallization and densitometric quantification, respectively. We
622 acknowledge computational and storage services (Maestro cluster) provided by the
623 Institut Pasteur IT Dept (Paris).

624 **Competing interests**

625 The authors declare no competing interests.

626 **References**

- 627 1. Wuichet, K., Cantwell, B.J. & Zhulin, I.B. Evolution and phyletic distribution of
628 two-component signal transduction systems. *Curr Opin Microbiol* **13**, 219-25
629 (2010).

- 630 2. Buschiazzo, A. & Trajtenberg, F. Two-Component Sensing and Regulation:
631 How Do Histidine Kinases Talk with Response Regulators at the Molecular
632 Level? *Annu Rev Microbiol* **73**, 22.1-22.22 (2019).
- 633 3. Gao, R., Bouillet, S. & Stock, A.M. Structural Basis of Response Regulator
634 Function. *Annu Rev Microbiol* **73**, 175-197 (2019).
- 635 4. Shinar, G., Milo, R., Martínez, M.R. & Alon, U. Input output robustness in
636 simple bacterial signaling systems. *Proc Natl Acad Sci U S A* **104**, 19931-5
637 (2007).
- 638 5. Gao, R. & Stock, A.M. Quantitative Kinetic Analyses of Shutting Off a Two-
639 Component System. *MBio* **8**(2017).
- 640 6. Siryaporn, A. & Goulian, M. Cross-talk suppression between the CpxA-CpxR
641 and EnvZ-OmpR two-component systems in *E. coli*. *Mol Microbiol* **70**, 494-
642 506 (2008).
- 643 7. Trajtenberg, F. et al. Regulation of signaling directionality revealed by 3D
644 snapshots of a kinase:regulator complex in action. *Elife* **5**(2016).
- 645 8. Saita, E. et al. A coiled coil switch mediates cold sensing by the
646 thermosensory protein DesK. *Mol Microbiol* **98**, 258-71 (2015).
- 647 9. Albanesi, D. et al. Structural plasticity and catalysis regulation of a
648 thermosensor histidine kinase. *Proc Natl Acad Sci U S A* **106**, 16185-90
649 (2009).
- 650 10. Casino, P., Miguel-Romero, L. & Marina, A. Visualizing autophosphorylation in
651 histidine kinases. *Nat Commun* **5**, 3258 (2014).

- 652 11. Casino, P., Rubio, V. & Marina, A. Structural insight into partner specificity
653 and phosphoryl transfer in two-component signal transduction. *Cell* **139**,
654 325-36 (2009).
- 655 12. Mechaly, A.E. et al. Structural Coupling between Autokinase and
656 Phosphotransferase Reactions in a Bacterial Histidine Kinase. *Structure* **25**,
657 939-944 e3 (2017).
- 658 13. Mechaly, A.E., Sassoon, N., Betton, J.M. & Alzari, P.M. Segmental helical
659 motions and dynamical asymmetry modulate histidine kinase
660 autophosphorylation. *PLoS Biol* **12**, e1001776 (2014).
- 661 14. Bourret, R.B. Receiver domain structure and function in response regulator
662 proteins. *Curr Opin Microbiol* **13**, 142-9 (2010).
- 663 15. Skerker, J.M. et al. Rewiring the specificity of two-component signal
664 transduction systems. *Cell* **133**, 1043-54 (2008).
- 665 16. Gushchin, I. et al. Mechanism of transmembrane signaling by sensor histidine
666 kinases. *Science* **356**(2017).
- 667 17. Molnar, K.S. et al. Cys-scanning disulfide crosslinking and bayesian modeling
668 probe the transmembrane signaling mechanism of the histidine kinase, PhoQ.
669 *Structure* **22**, 1239-1251 (2014).
- 670 18. Finn, R.D. et al. The Pfam protein families database: towards a more
671 sustainable future. *Nucleic Acids Res* **44**, D279-85 (2016).
- 672 19. Yamada, S. et al. Structure of PAS-linked histidine kinase and the response
673 regulator complex. *Structure* **17**, 1333-44 (2009).

- 674 20. Bilwes, A.M., Alex, L.A., Crane, B.R. & Simon, M.I. Structure of CheA, a signal-
675 transducing histidine kinase. *Cell* **96**, 131-41 (1999).
- 676 21. Rinaldi, J. et al. Structural Insights into the HWE Histidine Kinase Family: The
677 Brucella Blue Light-Activated Histidine Kinase Domain. *J Mol Biol* **428**, 1165-
678 1179 (2016).
- 679 22. Lassila, J.K., Zalatan, J.G. & Herschlag, D. Biological phosphoryl-transfer
680 reactions: understanding mechanism and catalysis. *Annu Rev Biochem* **80**,
681 669-702 (2011).
- 682 23. Meyerhof, O. & Shatas, R. Heat of hydrolysis of acetyl phosphate. *Archives of*
683 *Biochemistry and Biophysics* **40**, 253-262 (1952).
- 684 24. Garrison, A.W. & Boozer, C.E. The acid-catalyzed hydrolysis of a series of
685 phosphoramidates. *Journal of the American Chemical Society* **90**, 3486-3494
686 (1968).
- 687 25. Stock, J.B., Stock, A.M. & Mottonen, J.M. Signal transduction in bacteria. *Nature*
688 **344**, 395-400 (1990).
- 689 26. de Mendoza, D. Temperature sensing by membranes. *Annu Rev Microbiol* **68**,
690 101-16 (2014).
- 691 27. Aguilar, P.S., Hernandez-Arriaga, A.M., Cybulski, L.E., Erazo, A.C. & de
692 Mendoza, D. Molecular basis of thermosensing: a two-component signal
693 transduction thermometer in *Bacillus subtilis*. *EMBO J* **20**, 1681-91 (2001).
- 694 28. Trajtenberg, F. et al. Allosteric activation of bacterial response regulators: the
695 role of the cognate histidine kinase beyond phosphorylation. *MBio* **5**, e02105
696 (2014).

- 697 29. Trajtenberg, F., Grana, M., Ruetalo, N., Botti, H. & Buschiazzo, A. Structural
698 and enzymatic insights into the ATP binding and autophosphorylation
699 mechanism of a sensor histidine kinase. *J Biol Chem* **285**, 24892-903 (2010).
- 700 30. Morin, A. et al. Collaboration gets the most out of software. *Elife* **2**, e01456
701 (2013).
- 702 31. Tickle, I.J. et al. STARANISO ([http://staraniso.globalphasing.org/cgi-](http://staraniso.globalphasing.org/cgi-bin/staraniso.cgi)
703 [bin/staraniso.cgi](http://staraniso.globalphasing.org/cgi-bin/staraniso.cgi)). . *Cambridge, United Kingdom: Global Phasing Ltd.* (2018).
- 704 32. Calixto, A.R. et al. GTP Hydrolysis Without an Active Site Base: A Unifying
705 Mechanism for Ras and Related GTPases. *J Am Chem Soc* **141**, 10684-10701
706 (2019).
- 707 33. Cleland, W.W. & Hengge, A.C. Enzymatic mechanisms of phosphate and
708 sulfate transfer. *Chem Rev* **106**, 3252-78 (2006).
- 709 34. Quezada, C.M. et al. Structural and chemical requirements for histidine
710 phosphorylation by the chemotaxis kinase CheA. *J Biol Chem* **280**, 30581-5
711 (2005).
- 712 35. Marsico, F. et al. Multiscale approach to the activation and phosphotransfer
713 mechanism of CpxA histidine kinase reveals a tight coupling between
714 conformational and chemical steps. *Biochem Biophys Res Commun* **498**, 305-
715 312 (2018).
- 716 36. Trajtenberg, F. & Buschiazzo, A. Protein Dynamics in Phosphoryl-Transfer
717 Signaling Mediated by Two-Component Systems. *Methods Mol Biol* **2077**, 1-
718 18 (2020).

- 719 37. Imelio, J.A., Larrieux, N., Mechaly, A.E., Trajtenberg, F. & Buschiazzi, A.
720 Snapshots of the Signaling Complex DesK:DesR in Different Functional States
721 Using Rational Mutagenesis and X-ray Crystallography. *Bio-protocol* **7**, e2510
722 (2017).
- 723 38. Albanesi, D., Mansilla, M.C. & de Mendoza, D. The membrane fluidity sensor
724 DesK of *Bacillus subtilis* controls the signal decay of its cognate response
725 regulator. *J Bacteriol* **186**, 2655-63 (2004).
- 726 39. Huynh, T.N., Noriega, C.E. & Stewart, V. Conserved mechanism for sensor
727 phosphatase control of two-component signaling revealed in the nitrate
728 sensor NarX. *Proc Natl Acad Sci U S A* **107**, 21140-5 (2010).
- 729 40. Hentschel, E. et al. Phosphatase activity of the histidine kinases ensures
730 pathway specificity of the ChrSA and HrrSA two-component systems in
731 *Corynebacterium glutamicum*. *Mol Microbiol* **92**, 1326-42 (2014).
- 732 41. Lan, G., Sartori, P., Neumann, S., Sourjik, V. & Tu, Y. The energy-speed-
733 accuracy tradeoff in sensory adaptation. *Nat Phys* **8**, 422-428 (2012).
- 734 42. Batchelor, E. & Goulian, M. Robustness and the cycle of phosphorylation and
735 dephosphorylation in a two-component regulatory system. *Proc Natl Acad Sci*
736 *USA* **100**, 691-6 (2003).
- 737 43. Hart, Y. & Alon, U. The utility of paradoxical components in biological circuits.
738 *Mol Cell* **49**, 213-21 (2013).
- 739 44. Graham, D.L. et al. MgF(3)(-) as a transition state analog of phosphoryl
740 transfer. *Chem Biol* **9**, 375-81 (2002).

- 741 45. Schweins, T. et al. Substrate-assisted catalysis as a mechanism for GTP
742 hydrolysis of p21ras and other GTP-binding proteins. *Nat Struct Biol* **2**, 36-44
743 (1995).
- 744 46. Wylie, D., Stock, A., Wong, C.-Y. & Stock, J. Sensory transduction in bacterial
745 chemotaxis involves phosphotransfer between CHE proteins. *Biochemical*
746 *and Biophysical Research Communications* **151**, 891-896 (1988).
- 747 47. Woods, A.S. & Ferré, S. Amazing stability of the arginine-phosphate
748 electrostatic interaction. *J Proteome Res* **4**, 1397-402 (2005).
- 749 48. Maier, J.A. et al. ff14SB: Improving the Accuracy of Protein Side Chain and
750 Backbone Parameters from ff99SB. *J Chem Theory Comput* **11**, 3696-713
751 (2015).
- 752 49. Frisch, M. et al. Gaussian 09, Revision A. 01. *Gaussian, Inc.: Wallingford, CT*
753 (2009).
- 754 50. Götz, A.W., Clark, M.A. & Walker, R.C. An extensible interface for QM/MM
755 molecular dynamics simulations with AMBER. *J Comput Chem* **35**, 95-108
756 (2014).
- 757 51. Nitsche, M.A., Ferreria, M., Mocskos, E.E. & González Lebrero, M.C. GPU
758 Accelerated Implementation of Density Functional Theory for Hybrid
759 QM/MM Simulations. *J Chem Theory Comput* **10**, 959-67 (2014).
- 760 52. Zeida, A. et al. Molecular basis of the mechanism of thiol oxidation by
761 hydrogen peroxide in aqueous solution: challenging the SN2 paradigm. *Chem*
762 *Res Toxicol* **25**, 741-6 (2012).

- 763 53. Lopez, E.D. et al. Kinase Activation by Small Conformational Changes. *J Chem*
764 *Inf Model* **60**, 821-832 (2020).
- 765 54. Olivieri, F.A. et al. Conformational and Reaction Dynamic Coupling in
766 Histidine Kinases: Insights from Hybrid QM/MM Simulations. *J Chem Inf*
767 *Model* **60**, 833-842 (2020).
- 768 55. Unger, T., Jacobovitch, Y., Dantes, A., Bernheim, R. & Peleg, Y. Applications of
769 the Restriction Free (RF) cloning procedure for molecular manipulations and
770 protein expression. *J Struct Biol* **172**, 34-44 (2010).
- 771 56. Schneider, C.A., Rasband, W.S. & Eliceiri, K.W. NIH Image to ImageJ: 25 years
772 of image analysis. *Nat Methods* **9**, 671-5 (2012).
- 773 57. Vonrhein, C. et al. Data processing and analysis with the autoPROC toolbox.
774 *Acta Crystallogr D Biol Crystallogr* **67**, 293-302 (2011).
- 775 58. McCoy, A.J. et al. Phaser crystallographic software. *J Appl Crystallogr* **40**, 658-
776 674 (2007).
- 777 59. Emsley, P., Lohkamp, B., Scott, W.G. & Cowtan, K. Features and development
778 of Coot. *Acta Crystallogr D Biol Crystallogr* **66**, 486-501 (2010).
- 779 60. Bricogne, G. et al. BUSTER. 2.8.0. edn (Global Phasing Ltd. United Kingdom,
780 Cambridge, 2009).
- 781 61. Chen, V.B. et al. MolProbity: all-atom structure validation for macromolecular
782 crystallography. *Acta Crystallogr D Biol Crystallogr* **66**, 12-21 (2010).
- 783 62. Schrodinger, LLC. The PyMOL Molecular Graphics System, Version 1.8.
784 (2015).

- 785 63. Keller, S. et al. High-precision isothermal titration calorimetry with
786 automated peak-shape analysis. *Anal Chem* **84**, 5066-73 (2012).
- 787 64. Scheuermann, T.H. & Brautigam, C.A. High-precision, automated integration
788 of multiple isothermal titration calorimetric thermograms: new features of
789 NITPIC. *Methods* **76**, 87-98 (2015).
- 790 65. Houtman, J.C. et al. Studying multisite binary and ternary protein interactions
791 by global analysis of isothermal titration calorimetry data in SEDPHAT:
792 application to adaptor protein complexes in cell signaling. *Protein Sci* **16**, 30-
793 42 (2007).
- 794 66. Brautigam, C.A. Calculations and Publication-Quality Illustrations for
795 Analytical Ultracentrifugation Data. *Methods Enzymol* **562**, 109-33 (2015).
796

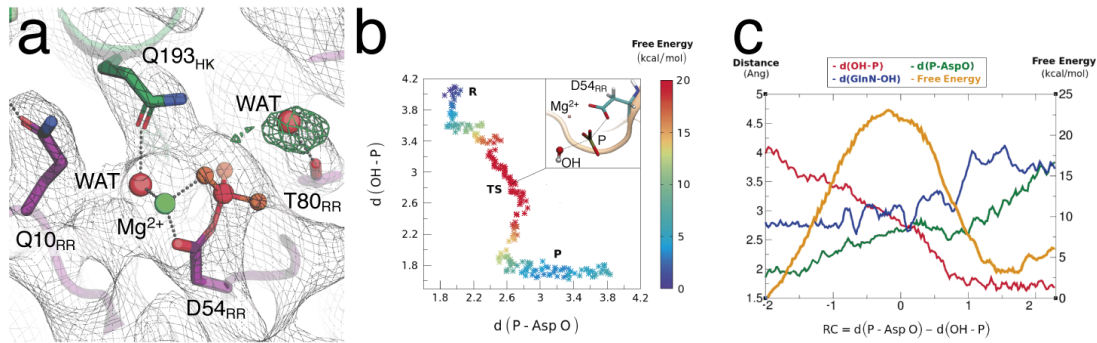
797

Table 1: Free energy derived from QM/MM calculations

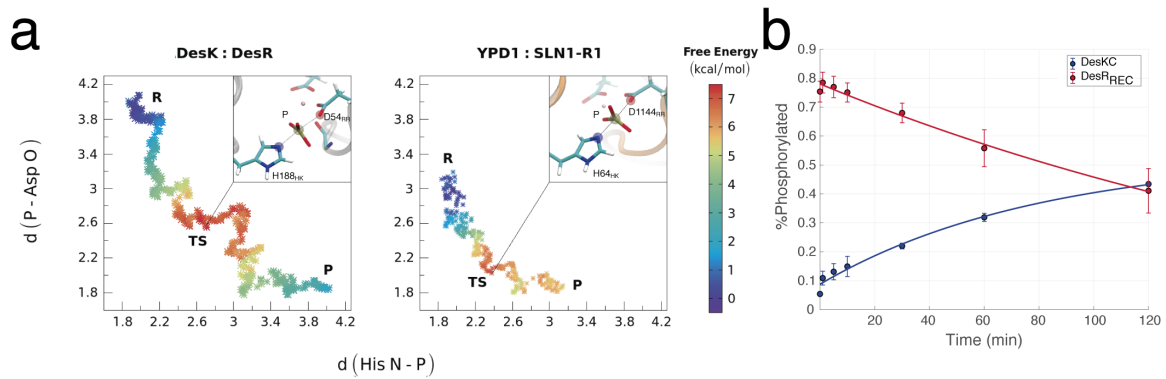
Phosphotransfer	ΔG^\ddagger (kcal/mol)	ΔG^0 (kcal/mol)
DesK:DesR	7.1	1.8
DesK:DesR (no Mg ²⁺)	19.4	8.2
DesK:DesR (T80A)	7.9	1.1
YPD1:SLN1-R1	7.1	4.8
His:Asp (water)	25.1	5.0

798

799

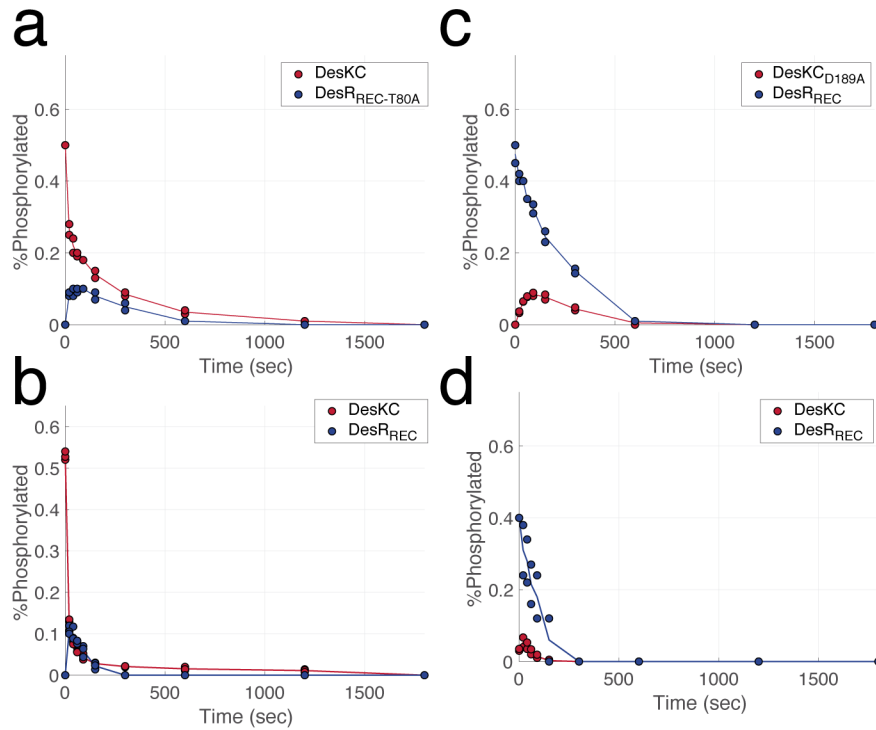


800 **Figure 1: HK phosphatase-catalyzed reaction.** a) Reaction center of the DesK-DesR
801 complex in the phosphatase state. The gray mesh shows 2mFobs-DFcalc electron
802 density map contoured at 1, and the green mesh shows positive peaks of the mFobs-
803 DFcalc electron density contour at 3.5. Key residues are depicted in sticks. b)
804 Bidimensional free energy diagram energy as a function of the bonds broken and
805 formed for the phosphatase reaction. The distance between the phosphorus atom of
806 the phosphoryl-moiety and the OE2 atom of D54_{RR} (P-Asp O) against the distance
807 between the phosphorus and hydroxyl anion (P-OH) is shown in the plot as a way of
808 describing the reaction path. Inset: QM region for QM-MM simulations of the
809 phosphatase reaction. c) Free Energy profile (orange) and main interatomic distances as
810 a function of the reaction coordinate for the phosphatase reaction, defined as the
811 difference between the P-Asp O distance and the OH-P distance.



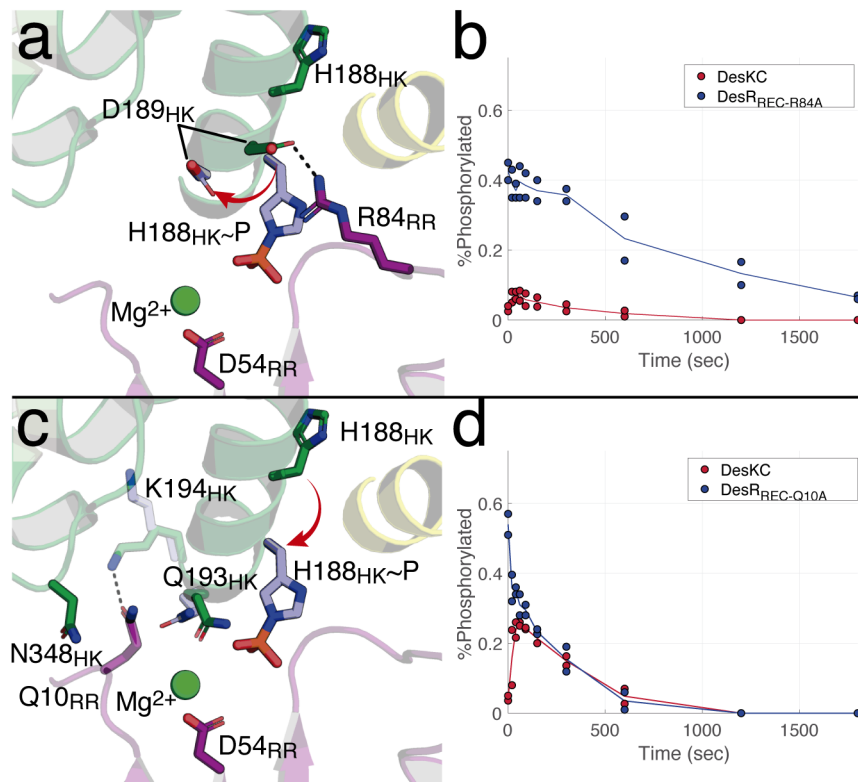
812

813 **Figure 2: Phosphoryl-transfer reaction.** a) Reaction diagram of the phosphoryl-
814 transfer reaction. The left panel shows the bidimensional free energy diagram energy as
815 function of the breaking and forming bonds of the DesK-DesR system (AspO-P vs
816 HisN-P). Right panel shows the Free Energy diagram for the reversible phosphorelay
817 Sln1-Ypd1 systems. b) Phosphotransfer kinetics in the absence of Mg²⁺. Equimolar
818 amounts of phosphorylated DesR_{REC} and DesKC were incubated and analyzed by
819 densitometry from Coomassie stained Phostag SDS-PAGE. The solid lines shows the
820 exponential fit of the phosphorylation degree of DesR-REC (red) and DesKC (blue).



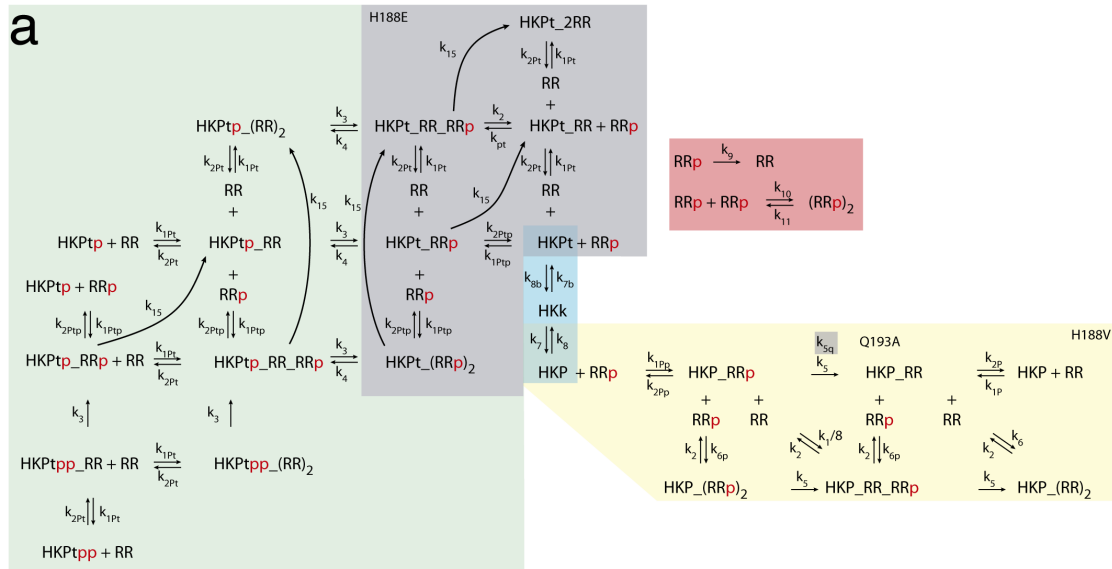
821

822 **Figure 3: Analysis of highly conserved residues in the phosphoryl-transfer**
823 **reaction.** Assays were performed with DesKC~P in the presence of DesR_{REC-T80A} (a) or
824 DesR_{REC} (b); or DesR_{REC}~P in the presence of DesKC_{D189A} (c) or DesKC (d). Degree of
825 phosphorylated of DesKC (red) and DesR_{REC} mutants (blue) was analyzed *in vitro* by
826 densitometry of Coomassie stained PhosTag SDS gels. Two independent experiments
827 are shown for each reaction.



828

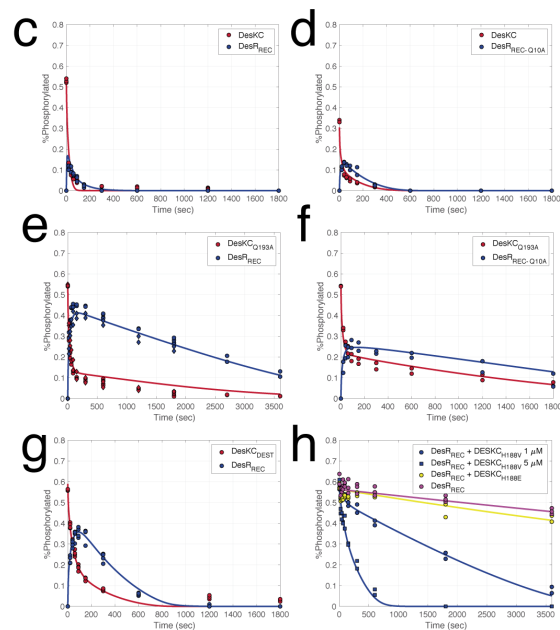
829 **Figure 4: Modulation of phosphoryl-transfer reversibility.** (a) Structural comparison
830 between the phosphotransferase (residues depicted in light blue) and phosphatase (in
831 green) complexes highlighting the interaction established by R84_{RR}. (b) Phosphoryl-
832 transfer assay showing the distribution of the phosphoryl-moiety between DesKC and
833 phosphorylated DesR_{REC-R84A}. (c) Similar view as in (a), showing Q10_{RR} inserted in a
834 pocket created at the ATP binding domain:DHp interface, and interacting with K194_{HK}.
835 (d) Phosphoryl-transfer assay of DesKC and phosphorylated DesR_{REC-Q10A}.



b

Table 2: Kinetic parameters

K_{phos} (k_4/k_3)	2.077E+01	2.517E-02
k_5 (s^{-1})	2.273E-01	2.720E-02
k_9 (s^{-1})	3.870E-04	1.323E-04
k_{10} (s^{-1})	2.923E-02	1.239E-03
$K_{D,RR}$ (μM)	3.324E-01	4.000E-04
K_{D2} (μM)	4.858E+01	6.500E-03
k_{6b} ($\mu M \cdot s^{-1}$)	1.708E-03	9.019E-04
k_{5q} (s^{-1})	6.082E-03	7.681E-04
k_6 ($\mu M \cdot s^{-1}$)	1.582E-01	3.826E-05
$K_{D,RR,Q193A}$ (μM)	1.442E+00	6.110E-02
$K_{D,HK,Q193A}$ (μM)	3.274E-01	3.620E-02
$k_{6bQ193A}$ ($\mu M \cdot s^{-1}$)	4.760E-06	3.281E-06
$K_{P \rightarrow K}$ (k_8/k_7)	3.661E-01	2.157E-02
$K_{K \rightarrow Pt}$ (k_{8b}/k_{7b})	8.755E+02	6.360E-01
$K_{P \rightarrow K(DEST)}$ (k_8/k_7)	1.873E-02	2.701E-03
$K_{P \rightarrow K(Q193A)}$ (k_8/k_7)	5.429E-02	9.747E-04
k_{6bp} ($\mu M \cdot s^{-1}$)	1.715E+01	5.243E-04
k_{6p} ($\mu M \cdot s^{-1}$)	3.392E+01	8.988E-02
$K_{P \rightarrow K(Q193A_AMP)}$ (k_8/k_7)	1.796E-01	1.660E-02



836

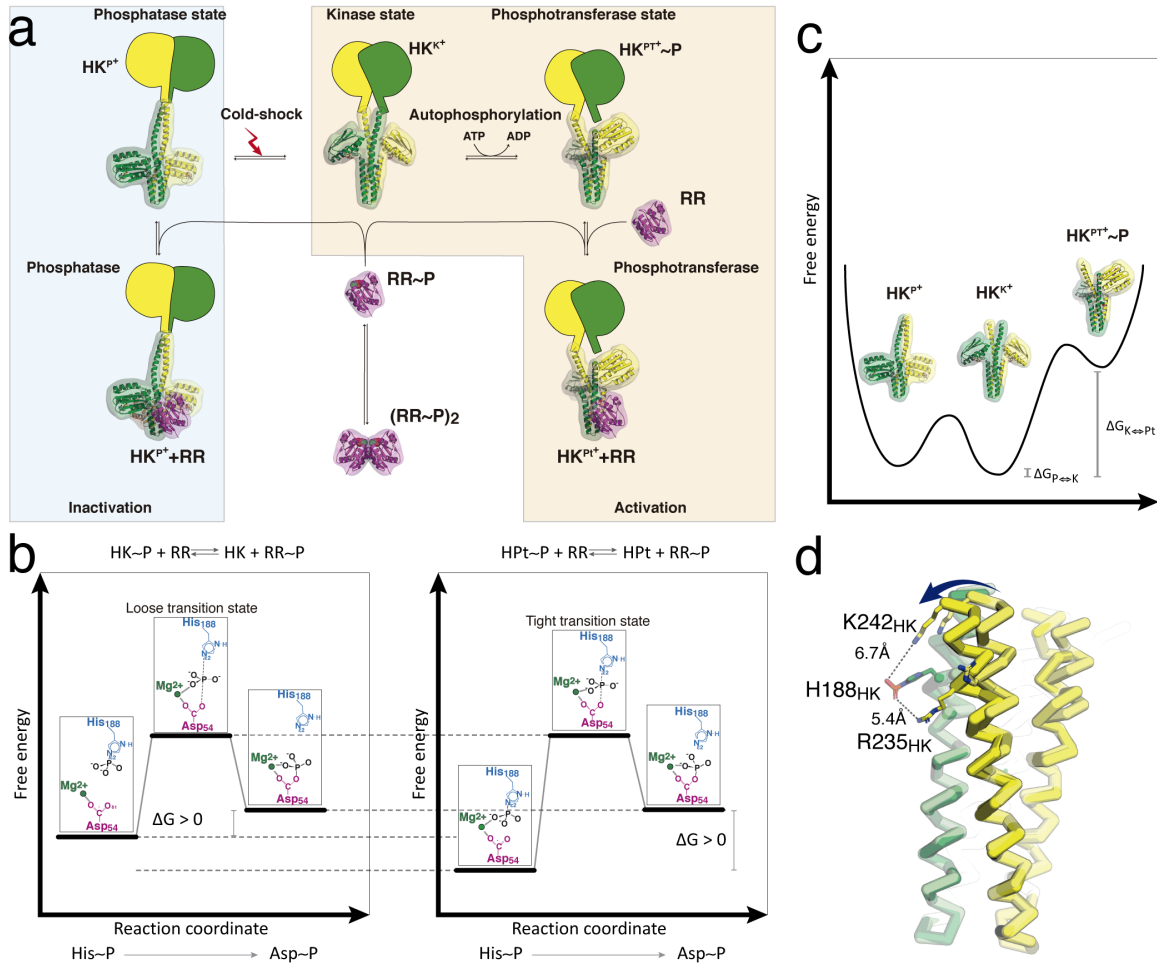
837 **Figure 5: Phosphoryl-transfer assay dataset and model fitting.** (a) Schematic
 838 representation of the kinetic model. Yellow shaded box are all the reactions involved in
 839 the HK-catalyzed dephosphorylation reaction (H188V module). The red box includes the
 840 dimerization and autodephosphorylation of the RR module. The gray box corresponds
 841 to the H188E module, which includes RR binding to the phosphotransferase, without
 842 phosphoryl-transfer reaction. Green box describes the phosphoryl-transfer reactions,

843 and in cyan the HK conformational transitions are represented. (b) Parameters of the
844 best fitted model. (c to g) Phosphoryl-transfer assays. The reactions were performed
845 using either DesR_{REC} (c, e and g) or DesR_{REC-Q10A} (d and f) and started with
846 phosphorylated wild type DesKC (c and d), DesKC_{Q193A} (e and f) or DesKC_{DEST} (g). (h)
847 Phosphatase assay incubating phosphorylated DesR_{REC} alone, with DesKC_{H188V} or
848 DesKC_{H188E}. The continuous trace (red and blue lines) depicts the prediction of the best-
849 fitted model.

850

851

852



853

854 **Figure 6:** DesK-DesR structural and kinetic model (a). b) Diagrammatic representation
 855 of the free energy transition of the phosphoryl-transfer reaction of a more loose (left
 856 panel) or tight (right panel) TS and the role of the Mg^{2+} . A shorter His-Asp distance
 857 places the phosphoryl moiety at interaction distance to the coordinated Mg^{+2} at the
 858 beginning of the reaction, thereby stabilizing the initial state c) Schematic
 859 representation of the conformational equilibrium of DesKC in the absence of
 860 phosphorylation, indicating the higher energy of the phosphotransferase state. d)
 861 Proposed role of $R235_{HK}$ and $K242_{HK}$ in sensing the phosphorylation state of the His.